Adaptive changes of presynaptic components in hippocampal CA1 subfield after transient global cerebral ischemia

Yan Zhang
Jilin University
Bai-Hong Tan
Jilin University Bethune College of Medicine: Jilin University Norman Bethune Health Science Center
Shuang Wu
Jilin University Bethune College of Medicine: Jilin University Norman Bethune Health Science Center
Cheng-Hao Wu
Jilin University Norman Bethune Health Science Center
Jia-Le Suo
Jilin University Norman Bethune Health Science Center
Yue Gui
Jilin University Norman Bethune Health Science Center
Yan-Chao Li (liyanchao@jlu.edu.cn)
College of Basic Medical Sciences, Norman Bethune Health Science Center of Jilin University
https://orcid.org/0000-0002-2884-9829

Research Article

Keywords: Dendritic spine, F-actin, synapsin I, transient cerebral ischemia, hippocampus

Posted Date: March 30th, 2021

DOI: https://doi.org/10.21203/rs.3.rs-330558/v1

Abstract

Transient global cerebral ischemia induces acute loss of dendritic spines of CA1 pyramidal neurons in the hippocampus. On the other hand, it is unclear how the presynaptic terminals, which had lost their postsynaptic contacts, are persistently preserved after ischemia. We modeled global cerebral ischemia with two-stage 4-vessel-occlusion in rats, and found that three postsynaptic markers, MAP2, PSD95, and F-actin, were all severely decreased in area CA1 after ischemia/reperfusion (I/R). No significant change was detected for synapsin I, a presynaptic marker, at the protein level in the CA1 region after I/R. However, the puncta size of synapsin I became slightly, but significantly reduced in the early stage of I/R. As time went on, the puncta number of synapsin I became moderately decreased, while the puncta size of synaspin I was significantly increased. Interestingly, some enlarged puncta of synapsin I were observed to terminate directly onto the dendritic shafts of CA1 pyramidal cells. Due to a severe decrease of F-actin in the dendritic spines, the ratio of synapsin I/F-actin puncta number became significantly increased after I/R. The decrease in puncta size of synapsin I in the early stage of I/R may be the result of excessive release of synaptic vesicles due to I/R-induced hyperexcitability in CA3 pyramidal cells, while the increase in puncta size of synapsin I in the later stage of I/R may reflect the disability of synaptic vesicle release due to the loss of postsynaptic contacts.

1. Introduction

As one of the main causes of death and disability in the elderly (Neumann et al. 2013), cardiopulmonary arrest also limits cerebral blood flow and leads to neuronal cell loss in specific brain regions (Hartman et al., 2005; Endres et al., 2008). Hippocampus is known as such a brain area that is exceedingly fragile to the ischemic attack. Studies using animal models showed that most pyramidal neurons in area CA1 of the hippocampus became dead from day 2 to 7 after transient global cerebral ischemia (Pulsinelli and Brierley 1979; Ruan et al. 2006).

Prior to the loss of CA1 neurons, extensive deletion of dendritic spines has been widely reported in the CA1 region (Johansen et al. 1984; Yamamoto et al. 1986; Kovalenko et al. 2006). In line with this observation, filamentous actin (F-actin) within the dendritic spines was progressively depolymerized in this region after global cerebral ischemia (Guo et al. 2019). As the only cytoskeletal component in the dendritic spines (Hotulainen and Hoogenraad 2010; Freire-Cobo et al. 2014), the destruction of F-actin inevitably leads to a volume collapse of the dendritic spines.

On the other hand, the temporal profile of ischemia-induced changes has not been fully clarified in the presynaptic terminals, which occupy the majority of the neuropil in the brain. Early ultrastructural studies show that the presynaptic boutons persisted in hippocampal CA1 region for several months after transient forebrain ischemia, despite cell death and dissolution of their postsynaptic contacts (Kirino 1982; Kirino et al. 1990; Bonnekoh et al. 1990). Consistently, immunohistochemical staining showed that synapsin I, a presynaptic marker, was spared or even increased in the CA1 subfield in ischemic animals or in glucose/oxygen deprived hippocampal slice (Kitagawa et al. 1992; Jung et al. 2004).

So far, most studies were focused primarily on the early dendritic injury and the delayed neuronal death, while less attention was paid to the possible effects of ischemia on the presynaptic components. Given the severe damage of dendritic spines, it is interesting to know whether or how the presynaptic terminals were preserved after ischemia/reperfusion (I/R). Such studies may provide key clues to understand the mechanisms underlying the reconstruction of neural connectivity after ischemia.

2. Materials And Methods

2.1 Induction of ischemia in rats

Two-month-old Wistar rats (male, 250 ~ 270g) were used to induce transient global cerebral ischemia with a four-vessel occlusion method (Pulsinelli and Brierley, 1979; Guo et al., 2019, Xiong et al., 2019). The animal experiments have been approved by the Animal Research Committee of Jilin University, and handled in accordance with the NIH Guide for the Care and Use of Laboratory Animals.

2.2 Sample preparations

For protein analysis, the CA1 region was micro-dissected from the hippocampi of sham-operated control and ischemic rats without fixation at day 2 and 7 after I/R.

For fluorescence analysis, day 1.5 after I/R was selected as a starting time point according to the results reported by Guo et al. (2019). The rats were fixed with 4% paraformaldehyde at day 1.5, 2, 3, 7 after I/R, and the brains were removed and cut into 30-μm-thick section, as described in our previous papers (Guo et al., 2019, Xiong et al., 2020).

2.3 Western blot analysis of microtubule-associated protein 2 (MAP2), postsynaptic density protein 95 (PSD95), and synapsin I in the CA1 subfield

The protein levels of MAP2, PSD95 and synapsin I in the CA1 region were detected with SDS electrophoresis and western blots. The primary antibodies used here included mouse anti-MAP2 monoclonal IgG (1:500, M9942, Sigma, USA), goat polyclonal anti-PSD95 IgG (ab12093, Abcam, USA), and rabbit polyclonal anti-synapsin I IgG (1:500, 51-5200, Thermo, USA). Monoclonal mouse anti-glyceraldehyde-3-phosphate dehydrogenase (GAPDH) IgM (1:1000, Boster, Wuhan, China) was used as a reference protein. ECL detection kit (Thermo, USA) was used to show protein bands, and western blot results were quantified using the Quantity One 4.6.6.

2.4 Determination of F-actin/G-actin (F/G) ratio in the CA1 subfield

F/G ratio was determined with an *in vivo* Assay Kit (BK037, Cytoskleton, USA). The bands of F- and G-actin were quantified with Quantity One 4.6.6, respectively, and the F/G ratio was further measured as previously described (Zhang et al., 2014; Xiong et al., 2018).

2.5 Fluorescence labeling of MAP2, synapsin I, and F-actin

MAP2, synapsin I and F-actin were stained in free-floating sections with mouse anti-MAP2 monoclonal IgG (1:500), rabbit polyclonal anti-synapsin I IgG (1:500), and Alexa 488-conjugated phalloidin (1:100), respectively. Alexa Fluor 488-conjugated donkey anti-mouse or donkey anti-rabbit IgG (Molecular Probes, Eugene, OR) was used to visualize mouse or rabbit primary antibodies. The staining procedure has been described in more detail in our previous papers (Xiong et al. 2015, 2019; Guo et al., 2019).

2.6 Dual fluorescence labeling

Dual fluorescence labeling was used to study the spatial relationships between different molecular markers in the CA1 region. The primary antibodies used here included mouse anti-MAP2 monoclonal IgG, rabbit polyclonal anti-synapsin I IgG, rabbit polyclonal anti-GFAP IgG (1:500, BA0056, Boster, Wuhan, China), and rabbit monoclonal anti-Iba1 IgG (ab178847, Abcam). The sections labeled with mouse anti-MAP2 or rabbit anti-synapsin I antibodies were further visualized with Alexa 488-conjugated donkey anti-mouse IgG (1:500) or Alexa 594-conjugated donkey anti-rabbit IgG (1:500). The sections labeled with rabbit anti-GFAP IgG or rabbit anti-Iba1 IgG were further visualized with Alexa 488-conjugated phalloidin (1:100) or Alexa 594-conjugated donkey anti-rabbit IgG. All reactions were carried out at room temperature, and the incubation time was controlled for about 2 hours.

2.7 Morphometric analyses

High resolution images were obtained with Olympus FV1000 laser scanning confocal microscope under Plan-Apo 60× oil immersion objective lens (1.42 NA, WD 0.15 mm). A method of morphometric analysis previously described by Rizk et al. (2014) was used to measure the number and size of positive structures in this study. Briefly, single-channel images of size 512× 512 were imported into Fiji software (http://imagej.nih.gov/ij), and analyzed with Squassh. The puncta number and size of positive structures were further analyzed with SPSS 18.0 (Chicago, IL, USA). Analysis of variance (ANOVA) was first performed to confirm whether the results were significant among different groups. Dunnett's multiple comparison test was then used to detect the differences between the control and experimental groups.

3. Results

3.1 Ischemia-induced changes of postsynaptic components in the CA1 subfield

Relative to sham-operated control rats, the protein levels of MAP2 and PSD95 were significantly reduced in the CA1 subfield in ischemic animals at day 2 and 7 after I/R (Fig. 1A and 1B). Similarly, the ratio of F/G in the CA1 subfield was reduced from 0.84 in sham-operated controls to 0.61 and 0.37 in ischemic animals at day 2 and 7 after I/R, respectively (Fig. 1C).

Under the conventional fluorescence microscope, the positive signals for MAP2 or F-actin were distributed throughout the hippocampus except for the layers containing neuronal cell bodies in sham-operated control rats (Fig. 2A and 2F). After I/R, MAP2 and F-actin were both selectively lost in the CA1 subfield in

ischemic animals from day 2 (Fig. 2C and 2G), and became progressively severe over time (Fig. 2D-2E, and 3C-3D).

Under the laser scanning confocal microscope, MAP was distributed in the proximal and distal dendrites of CA1 pyramidal cells (Fig. 2A and 2E), while F-actin was located predominantly in the dendritic spines of CA1 pyramidal cells in sham-operated control rats (Fig. 2A1). Double fluorescence labeling revealed little overlapping between F-actin and MAP2 (Fig. 3A2).

After I/R, MAP2 first disappeared from the distal branches, and finally from the proximal branches of the dendrites (Fig. 2B, 2C, and 2D), and few fluorescence signals for MAP2 were detected in the CA1 stratum radiatum in the later stage of I/R (Fig. 3D). As previously described by Guo et al. (2019), global cerebral ischemia induced progressive decrease in F-actin in the dendritic spines, but the F-actin in the dendrites was dramatically increased at day 1.5 and 2 (Fig. 2B1, 2C1, 3B2 and 3C2). The F-actin-positive dendrites eventually disappeared in CA1 stratum radiatum, but some tubular or circular structures, which were positively labeled for both F-actin and microglial Iba1 (Fig. 4), became prominent in this region (Fig. 3D1).

The content of F-actin in microglia was very low in the sham-operated control and ischemic animals in the early stage of I/R, probably due to the small number and size of rest microglia (Fig. 4A, 4A1 – 4A2, and 4B1). From day 3 to 7 after I/R, microglia were dramatically increased in both number and size, and F-actin was concomitantly increased in the microglia (Fig. 4C – 4D, and 4C1-4D1). F-actin was localized predominantly in the peripheral cytoplasm of activated microglia, showing circular or tubular shapes (Fig. 4C2-4D2).

Quantitative analysis showed that the puncta number of F-actin per unit area was significantly decreased in CA1 stratum radiatum in ischemic animals at day 1.5 after I/R (Figs. 5B, 5B1, and 5F), but the area fraction of F-actin was not significantly changed at this time point (Fig. 5C), relative to sham-operated control rats (Fig. 5A and 5A1). Due to the aggregation of F-actin into threadlike structures, the mean size of F-actin-positive structures became much larger in ischemic animals (Figs. 5B, 5B, and 5G).

The puncta number per unit area and the area fraction of F-actin became progressively reduced in the CA1 stratum radiatum in ischemic animals from day 2 to 7 after I/R (Fig. 5C-5E, and 5C1-5E1), while the mean size of F-actin-positive structures became significantly increased from day 2 to 7 (Fig. 5G). Since F-actin in microglia was not excluded from the quantitative analysis, the number of the remaining dendritic spines was much lower than that measured by counting the F-actin puncta, especially in the later stage of I/R.

3.2 Ischemia-induced change of presynaptic components in CA1 stratum radiatum

Relative to sham-operated control rats, no significant change was detected for synapsin I at the protein level in the CA1 subfield in ischemic animals (Fig. 1D).

Under the conventional fluorescence microscope, synapsin I was evenly distributed throughout the hippocampus except for the pyramidal cell bodies and their dendrites (Fig. 2K). Relative to sham-operated

control rats, the conventional fluorescence microscopy did not reveal any remarkable changes of synaspin I in either fluorescence intensity or staining pattern within the first week following ischemia (Fig. 2L -2O).

Under the laser scanning confocal microscope, the positive signals for synapsin I was observed as discrete dots in CA1 stratum radiatum (Fig. 3E1). The dendrites, which contained no synapsin I in their cytoplasm, exhibited “silhouettes” due to negative staining (Fig. 3E, 3E1, and 3E2).

In ischemic rats, the punctate labeling of synapsin I became slightly sparse in CA1 stratum radiatum from day 2 after I/R, while the sizes of synapsin I-positive puncta were remarkably increased from day 2 after I/R (Fig. 3F1-3H1). At day 1.5 after I/R, quantitative analysis showed that synapsin I was not significantly changed in puncta number in ischemic animals (Figs. 5J, 5J1, and 5N), relative to the sham-operated control (Fig. 5I and 5I1). However, the puncta size of synapsin I became significantly reduced at this time point (Fig. 5O) so that the area fraction of synapsin I became significantly decreased (Fig. 5P).

From day 2 to 7 after I/R, the puncta number of synapsin I per unit area became significantly reduced in CA1 stratum radiatum in ischemic animals (Figs. 5K-5M, 5K1-5M1, and 5O). However, due to the increased puncta size, the mean area fraction of synaspin I was not significantly changed in CA1 stratum radiatum in ischemic animals (Fig. 5P), relative to the sham-operated control. Due to the more significant decrease of F-actin in puncta number, the ratio of synapsin I/F-actin puncta number became significantly increased from day 1.5 to 7 after I/R (Fig. 5G).

Since some dendrites could still be identified due to the uneven labeling for MAP2 in their shafts (Fig. 3F and 3G), many large puncta of synapsin I were found terminating onto the shafts of these dendrites (arrows in Fig. 3F2-G2).

4. Discussion

Transient global cerebral ischemia results in delayed neuronal death in the CA1 subfield of hippocampus within the first week in rats and gerbils (Pulsinelli and Brierley 1979; Ruan et al. 2006). As compared with the delayed neuronal death, dendritic spines of the damaged neurons collapsed rapidly after I/R, due to a rapid depolymerization of their F-actin network (Guo et al. 2018; Xiong et al. 2018).

F-actin is highly fragile to ATP-depleted conditions because 50% of the ATP in neurons is used to maintain the F-actin network (Bernstein and Bamburg 2003). Interestingly, F-actin was not simply depolymerized in the impaired neurons, but aggregated into threadlike structures in the distal or the proximal dendrites in the early stage of I/R. This ectopic aggregation was first described in ischemic rats by us (Guo et al. 2019), but a similar phenomenon has already been documented in cultured neurons after oxygen and glucose deprivation (Gisselsson et al. 2005, 2010). Treatment with F-actin-depolymerizing drugs such as latrunculins significantly reduced the actin aggregates in size in cultured neurons after oxygen/glucose deprivation, but could not prevent the formation of F-actin aggregates, indicating that not all the F-actin in the aggregates were newly formed (Gisselsson et al. 2010).

F-actin in the dendritic spines is anchored at the base of spines to microtubules in the dendrites (Korobova and Svitkina 2010; Gu et al. 2008). Prior to neuronal death, microtubules were depolymerized after ischemia (Xiong et al., 2019). Probably due to the loss of anchorage provided by microtubules, a pool of F-actin in the dendritic spine, which was resistant to ATP depletion (Forscher and Smith 2003), might recede from the dendritic spines into the trunk of their parent dendrites. In support of this, F-actin aggregation in the dendrites occurred just at the sites where spines have collapsed, and the amount of aggregating F-actin was proportional to the number of spines that had collapsed (Gisselsson et al. 2005, 2010).

So far, the damage to the dendritic spines induced by ischemia have attracted considerable attention, while there are few studies on the presynaptic changes in the ischemic brain. This may be partially due to the fact that previous immunohistochemical and ultrastructural studies reported that the presynaptic terminals were relatively resistant to the ischemic stress ((Kirino 1982; Kirino et al. 1990; Bonnekoh et al. 1990; Kitagawa et al. 1992; Jung et al. 2004). The persistence of presynaptic terminals without their target neurons seems surprising, however, the resolution of fluorescence micrographs provided by previous studies is too low to distinguish the subcellular changes of synapsin I in the CA1 subfield I after ischemia.

Similarly, we did not find any remarkable alterations of synapsin I in ischemic rats by conventional fluorescence microscopy. Differently, our confocal microscopic observations revealed that the number and size of synapsin I puncta were significantly changed in CA1 stratum radiatum after ischemia. In the early stage of I/R, the puncta size of synapsin I, rather than the puncta number, became significantly reduced. This may be due to increased synaptic transmission in the ischemic brain areas, since ultramicroscopical and ultrastructural observations demonstrated a considerable reduction of synaptic vesicles in the active zone in the early stage of I/R (von Lubitz and Diemer 1983; Kovalenko et al. 2006). Consistently, the increased synaptic transmission via glutaminergic Schaffer collaterals of CA3 neurons has been hypothesized to cause the delayed neuronal death in the CA1 subfield (von Lubitz and Diemer 1983; Kovalenko et al. 2006).

According to our observations, the puncta number of synapsin I per unit area was moderately reduced from day 2 to 7 after I/R, but the puncta size of synapsin I was remarkably increased so that the mean area fraction of synaspin I in CA1 stratum radiatum was not significantly different between the sham-operated and ischemic animals. Interestingly, many large puncta of synapsin I were observed terminating directly onto the dendritic shafts in CA1 stratum radiatum. Since the ratio of synapsin I/F-actin puncta number was significantly increased, quite a few synapsin I-positive puncta were solitary terminals without postsynaptic contacts. To our knowledge, these presynaptic changes have not been reported in ischemic animals before.

Of relevance to our observations, several reports have documented the immunohistochemical changes of other presynaptic proteins, such as SNAP-25 and SVP-38, in the hippocampus after global cerebral ischemia (Miyazawa et al. 1995; Ishimaru et al. 2001). In gerbils which underwent 5-min bilateral carotid

artery ligature, Ishimaru et al (2001) found that SNAP-25 immunoreactivity in CA1 stratum radiatum was not changed at day 1, but significantly decreased from day 2 after I/R. By using the same ischemia model, Miyazawa et al. (1995) reported that immunostaining against SVP-38 became diffuse and weak in the CA1 subfield at day 1. Although they did not examine the ischemic animals at day 2 or 3, Miyazawa et al. (1995) found that SVP-38 immunoreactivity was restored to a control level after day 4 after I/R. Similar to ours, the two studies reported that both SNAP-25 and SVP-38 immunoreactivity gave a 'coarse' appearance with increased size in the CA1 subfield in the ischemic animals at day 7.

The pathologic role of the enlarged solitary presynaptic endings is unclear. The axonal terminals projecting to CA1 neurons are derived from the Schaffer collaterals of CA3 neurons, which remained largely intact after ischemia. Therefore, the stimulus for the increased synapsin-I immunoreactivity in the presynaptic terminals may be the death of CA1 cells and the loss of dendritic spines. As a necessary component of presynaptic terminals, synapsin I is indispensable for neurotransmitter release by reversibly tethering synaptic vesicles to actin (Zhang et al. 2018). Therefore, the enlargement of synapsin-I puncta might be the result of the decrease of neurotransmitter release due to the loss of postsynaptic components. Since synaptic transmission was severely impaired, it could be expected that the synaptic vesicles might be accumulated in the presynaptic terminals.

In addition to neurotransmitter release, induction of synapsin-I expression has been observed as a consequence of presynaptic nerve maturation and remodeling, which occurs during development or following lesion-induced plasticity in adulthood (Ferreira et al. 1998). In the middle portion of stratum radiatum, almost all the presynaptic terminals from afferent Schaffer colatterals of CA3 pyramidal cells terminate on the dendritic spines of CA1 pyramidal cells forming excitatory synapses, while the number of those terminating onto the dendritic shafts are less than 3% (Megías et al. 2001). After I/R, we observed that many enlarged puncta of synapsin I were terminating directly onto the shafts of dendrites. The undying mechanisms remain to clarify, but it is quite likely that the remaining presynaptic terminals might have undergone some remodeling to find new postsynaptic counterparts for their lost connections.

5 Conclusion

This study examined the ischemia-induced changes in both the pre- and post-synaptic regions in CA1 stratum radiatum. Consistent with the severe damage of postsynaptic components, significant changes were also observed in the presynaptic regions, including the decrease in number and the increase in size of synapsin I puncta. This study provides new important clues for understanding the ischemia-induced adaptive changes in the brain.

Declarations

Fund

This work was supported by National Natural Science Foundation of China (General Program), grant number: 81871014 (to YC Li).

CONFLICT OV INTEREST

None of the authors has any conflict of interest to disclose.

DATA AVAILABILITY STATEMENT

The experimental data in this study can be obtained upon request to the corresponding author.

Authors' contributions

Y.C. Li conceived and designed the study. Y. Zhang and B.H. Tan performed the experiment. Zhang Y and Tan B.H. Tan equally contributed to this work: Investigation, Validation, Writing. Wu S. and Wu C.H.: Software, Formal analysis, Writing. Suo J.L. and Gui Y.: Software, Formal analysis. All authors critically reviewed and approved the final version of the paper.

Ethics approval

The experimental procedures adhered to the ethical principles of experiments on animals of Jilin University, and were approved by the Animal Research Committee of Jilin University (Permit Number: SYXK□Ji□2017-0003).

References

1. Bernstein BW, Bamburg JR (2003) Actin-ATP hydrolysis is a major energy drain for neurons. J Neurosci 23:1–6. doi:10.1523/JNEUROSCI.23-01-00002.2003
2. Bonnekoh P, Barbier A, Oschlies U, Hossmann KA (1990) Selective vulnerability in the gerbil hippocampus: morphological changes after 5-min ischemia and long survival times. Acta Neuropathol 80:18–25. doi:10.1007/BF00294217
3. Buddle M, Eberhardt E, Ciminello LH, Levin T, Wing R, DiPasquale K, Raley-Susman KM (2003) Microtubule-associated protein 2 (MAP2) associates with the NMDA receptor and is spatially redistributed within rat hippocampal neurons after oxygen-glucose deprivation. Brain Res 978:38–50. doi:10.1016/s0006-8993(03)02758-6
4. Capani F, Ellisman MH, Martone ME (2001) Filamentous actin is concentrated in specific subpopulations of neuronal and glial structures in rat central nervous system. Brain Res 923:1–11. doi:10.1016/s0006-8993(01)03189-4
5. Dawson DA, Hallenbeck JM (1996) Acute focal ischemia-induced alterations in MAP2 immunostaining: description of temporal changes and utilization as a marker for volumetric assessment of acute brain injury. J Cereb Blood Flow Metab 16:170–174. doi:10.1097/00004647-199601000-00020

6. Dillon C, Goda Y (2005) The actin cytoskeleton: integrating form and function at the synapse. Annu Rev Neurosci 28:25–55. doi:10.1146/annurev.neuro.28.061604.135757
7. Endres M, Engelhardt B, Koistinaho J, Lindvall O, Meairs S, Mohr JP, Planas A, Rothwell N, Schwaninger M, Schwab ME, Vivien D, Wieloch T, Dirnagl U (2008) Improving outcome after stroke: overcoming the translational roadblock. Cerebrovasc Dis 25:268–278. doi:10.1159/000118039
8. Fath KR, Lasek RJ (1988) Two classes of actin microfilaments are associated with the inner cytoskeleton of axons. J Cell Biol 107:613–621. doi:10.1083/jcb.107.2.613
9. Ferreira A, Chin LS, Li L, Lanier LM, Kosik KS, Greengard P (1998) Distinct roles of synapsin I and synapsin II during neuronal development. Mol Med 41:22–28
10. Forscher P, Smith SJ (1988) Actions of cytochalasins on the organization of actin filaments and microtubules in a neuronal growth cone. J Cell Biol 107:1505–1516. doi:10.1083/jcb.107.4.1505
11. Freire-Cobo C, Sierra-Paredes G, Freire M, Sierra-Marcuño G (2014) The calcineurin inhibitor Ascomicin interferes with the early stage of the epileptogenic process induced by Latrunculin A microperfusion in rat hippocampus. J Neuroimmune Pharmacol 9:654–667. doi:10.1007/s11481-014-9558-9
12. Fifková E (1985) Actin in the nervous system. Brain Res 356:187–215
13. Fukaya M, Watanabe M (2000) Improved immunohistochemical detection of postsynaptically located PSD-95/SAP90 protein family by protease section pretreatment: a study in the adult mouse brain. J Comp Neurol 426:572–586
14. Gisselsson LL, Matus A, Wieloch T (2005) Actin redistribution underlies the sparing effect of mild hypothermia on dendritic spine morphology after in vitro ischemia.J Cereb. Blood Flow Metab 25:1346–1355. doi:10.1038/sj.jcbfm.9600131
15. Gisselsson L, Toresson H, Ruscher K, Wieloch T (2010) Rho kinase inhibition protects CA1 cells in organotypic hippocampal slices during in vitro ischemia. Brain Res 1316:92–100. doi:10.1016/j.brainres.2009.11.087
16. Gu J, Firestein BL, Zheng JQ (2008) Microtubules in dendritic spine development. J Neurosci 28:12120–12124. doi:10.1523/JNEUROSCI.2509-08.2008
17. Guo CY, Xiong TQ, Tan BH, Gui Y, Ye N, Li SL, Li YC (2019) The temporal and spatial changes of actin cytoskeleton in the hippocampal CA1 neurons following transient global ischemia. Brain Res 1720:146297. doi:10.1016/j.brainres.2019.06.016
18. Hartman RE, Lee JM, Zipfel GJ, Wozniak DF (2005) Characterizing learning deficits and hippocampal neuron loss following transient global cerebral ischemia in rats. Brain Res 1043:48–56. doi:10.1016/j.brainres.2005.02.030
19. Hotulainen P, Hoogenraad CC (2010) Actin in dendritic spines: connecting dynamics to function. J Cell Biol 189:619–629. Doi:10.1083/jcb.201003008
20. Ishimaru H, Casamenti F, Uéda K, Maruyama Y, Pepeu G (2001) Changes in presynaptic proteins, SNAP-25 and synaptophysin, in the hippocampal CA1 area in ischemic gerbils. Brain Res 903:94–101. doi:10.1016/s0006-8993(01)02439-8

21. Johansen FF, Jørgensen MB, Ekström von Lubitz DK, Diemer NH (1984) Selective dendrite damage in hippocampal CA1 stratum radiatum with unchanged axon ultrastructure and glutamate uptake after transient cerebral ischaemia in the rat. Brain Res 291:373–377
22. Jung YJ, Park SJ, Park JS, Lee KE (2004) Glucose/oxygen deprivation induces the alteration of synapsin I and phosphosynapsin. Brain Res 996:47–54. doi:10.1016/j.brainres.2003.09.069
23. Kirino T (1982) Delayed neuronal death in the gerbil hippocampus following ischemia. Brain Res 239:57–69. doi:10.1016/0006-8993(82)90833-2
24. Kirino T, Tamura A, Sano K (1990) Chronic maintenance of presynaptic terminals in gliotic hippocampus following ischemia. Brain Res 510:17–25. doi:10.1016/0006-8993(90)90722-n
25. Kitagawa K, Matsumoto M, Sobue K, Tagaya M, Okabe T, Niinobe M, Ohtsuki T, Handa N, Kimura K, Mikoshiba K et al (1992) The synapsin I brain distribution in ischemia. Neuroscience 46:287–299. doi:10.1016/0306-4522(92)90051-3
26. Korobova F, Svitkina T (2010) Molecular architecture of synaptic actin cytoskeleton in hippocampal neurons reveals a mechanism of dendritic spine morphogenesis. Mol Biol Cell 21:165–176. doi:10.1091/mbc.e09-07-0596
27. Kovalenko T, Osadchenko I, Nikonenko A, Lushnikova I, Voronin K, Nikonenko I, Muller D, Skibo G (2006) Ischemia-induced modifications in hippocampal CA1 stratum radiatum excitatory synapses. Hippocampus 16:814–825. doi:10.1002/hipo.20211
28. Megías M, Emri Z, Freund TF, Gulyás AI (2001) Total number and distribution of inhibitory and excitatory synapses on hippocampal CA1 pyramidal cells. Neuroscience 102:527–540. doi:10.1016/s0306-4522(00)00496-6
29. Miyazawa T, Sato K, Obata K (1995) A synaptic vesicle-associated protein (SVP-38) as an early indicator of delayed neuronal death. J Cereb Blood Flow Metab 15:462–466. doi:10.1038/jcbfm.1995.57
30. Morris JR, Lasek RJ (1984) Monomer-polymer equilibria in the axon: direct measurement of tubulin and actin as polymer and monomer in axoplasm. J Cell Biol 98:2064–2076. doi:10.1083/jcb.98.6.2064
31. Neumann JT, Cohan CH, Dave KR, Wright CB, Perez-Pinzon MA (2013) Global cerebral ischemia: synaptic and cognitive dysfunction. Curr Drug Targets 14:20–35. doi:10.2174/138945013804806514
32. Ouyang Y, Yang XF, Hu XY, Erbayat-Altay E, Zeng LH, Lee JM, Wong M (2007) Hippocampal seizures cause depolymerization of filamentous actin in neurons independent of acute morphological changes. Brain Res 1143:238–246. doi:10.1016/j.brainres.2007.01.077
33. Pulsinelli WA, Brierley JB (1979) A new model of bilateral hemispheric ischemia in the unanesthetized rat. Stroke 10:267–272
34. Rizk A, Paul G, Incardona P, Bugarski M, Mansouri M, Niemann A, Ziegler U, Berger P, Sbalzarini IF (2014) Segmentation and quantification of subcellular structures in fluorescence microscopy images using Squassh. Nat Protoc 9:586–596. doi:10.1038/nprot.2014.037

35. Ruan YW, Lei Z, Fan Y, Zou B, Xu ZC (2009) Diversity and fluctuation of spine morphology in CA1 pyramidal neurons after transient global ischemia. J Neurosci Res 87:61–68. doi:10.1002/jnr.21816
36. von Lubitz DK, Diemer NH (1983) Cerebral ischemia in the rat: ultrastructural and morphometric analysis of synapses in stratum radiatum of the hippocampal CA-1 region. Acta Neuropathol 61:52–60. doi:10.1007/BF00688386
37. Xiong TQ, Chen LM, Tan BH, Guo CY, Li YN, Zhang YF, Li SL, Zhao H, Li YC (2018) The effects of calcineurin inhibitor FK506 on actin cytoskeleton, neuronal survival and glial reactions after pilocarpine-induced status epilepticus in mice. Epilepsy Res 140:138–147. doi:10.1016/j.eplepsyres.2018.01.007
38. Xiong TQ, Guo CY, Tan BH, Gui Y, Li YC (2019) The temporal and spatial changes of microtubule cytoskeleton in the CA1 stratum radiatum following global transient ischemia. J Chem Neuroanat 101:101682. doi:10.1016/j.jchemneu.2019.101682
39. Xiong TQ, Guo CY, Tan BH, Gui Y, Li YC (2019) The temporal and spatial changes of microtubule cytoskeleton in the CA1 stratum radiatum following global transient ischemia. J Chem Neuroanat 101:101682. doi:10.1016/j.jchemneu.2019.101682
40. Yamamoto K, Morimoto K, Yanagihara T (1986) Cerebral ischemia in the gerbil: transmission electron microscopic and immunoelectron microscopic investigation. Brain Res 384:1–10
41. Zeng LH, Xu L, Rensing NR, Sinatra PM, Rothman SM, Wong M (2007) Kainate seizures cause acute dendritic injury and actin depolymerization in vivo. J Neurosci 27:11604–11613. doi:10.1523/JNEUROSCI.0983-07.2007
42. Zhang N, Zhu H, Han S, Sui L, Li J (2018) cPKCγ alleviates ischemic injury through modulating synapsin Ia/b phosphorylation in neurons of mice. Brain Res Bull 142:156–162. doi:10.1016/j.brainresbull.2018.07.005
43. Zhang YF, Xiong TQ, Tan BH, Song Y, Li SL, Yang LB, Li YC (2014) Pilocarpine-induced epilepsy is associated with actin cytoskeleton reorganization in the mossy fiber-CA3 synapses. Epilepsy Res 108:379–389. doi:10.1016/j.eplepsyres.2014.01.016

Figures

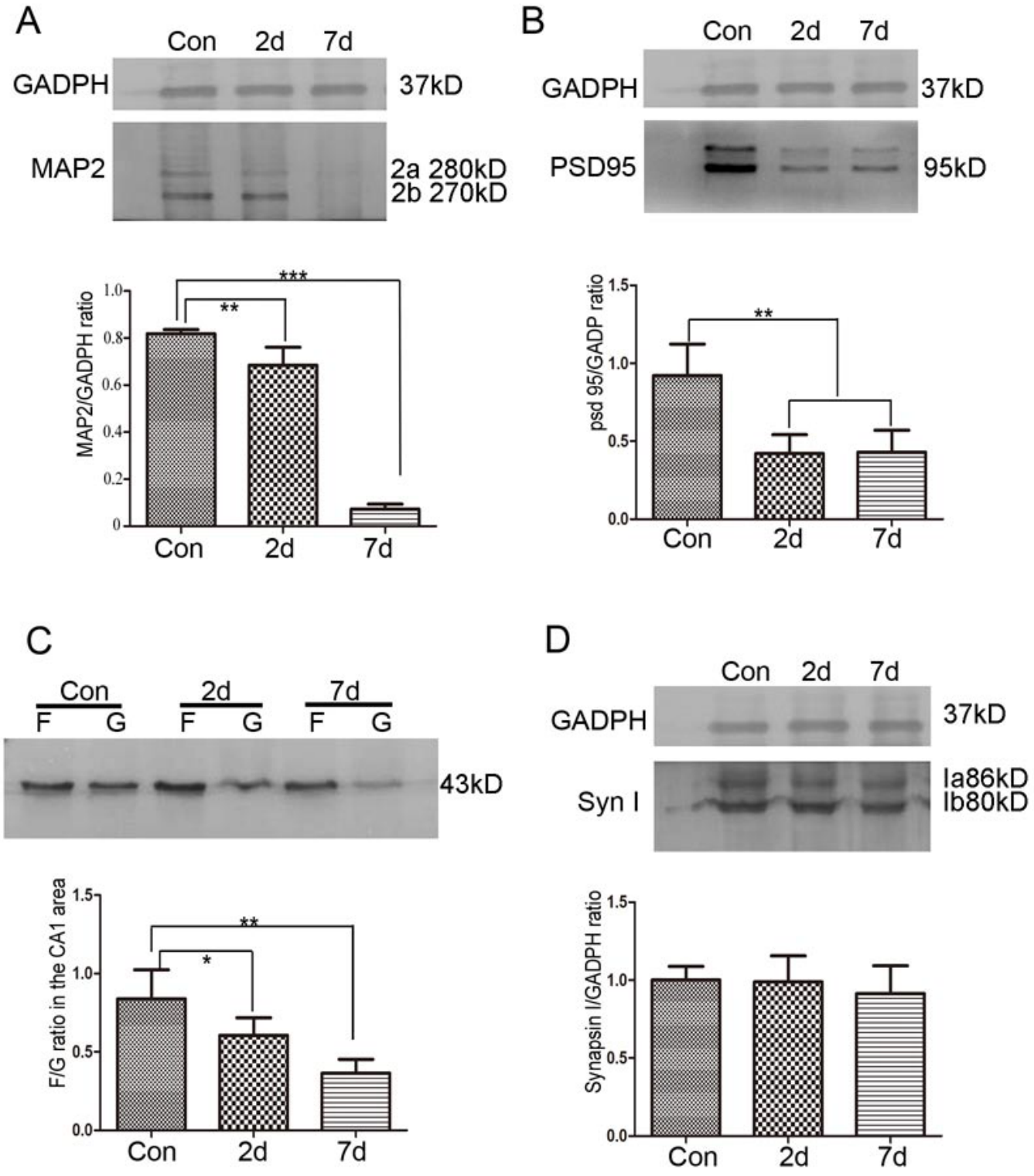

Figure 1

Western blot analysis of MAP2 (A), PSD95 (B), F/G ratio (C), and synapsin I (D) in microdissected CA1 subfield after transient global cerebral ischemia. Summarized western blot data show that the protein levels of MAP2, PSD95 and F/G ratio are significantly decreased in ischemic animals on days 2 and 7 after I/R, relative to the sham-operated control group, whereas no significant change of synapsin I is

detected in the CA1 subfield after I/R (*P<0.05, **P < 0.01, ***P < 0.001, n=6 per group, Error bars represent SEM.)

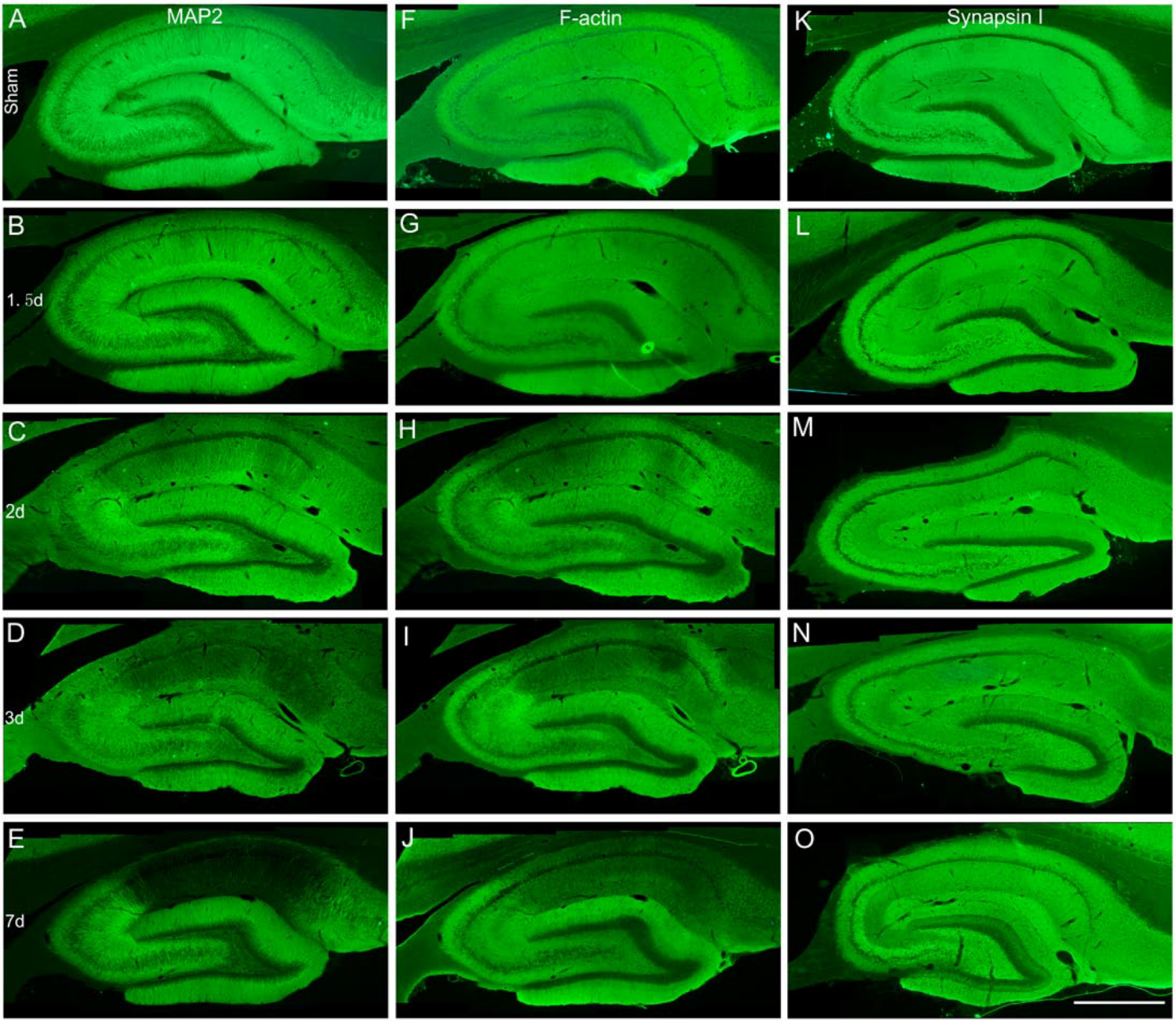

Figure 2

Immunofluorescence staining of MAP2 (A-E), F-actin (F-J) and synapsin I (K-O) in the hippocampus after transient global cerebral ischemia. Scale Bars: A-U, 500 μm. Sham-operated control and different ischemic groups are labeled in the left-most column. The fluorescence signals of MAP2 (A), and F-actin (F) are distributed homogeneously throughout the hippocampus in sham-operated control rats. No remarkable change in fluorescence staining of MAP2 or F-actin is observed at day 1.5 after I/R (B). From day 2 after I/R, a dramatic loss of MAP2 (C-E) or F-actin (H-J) is observed in the CA1 subfield in ischemic rats, relative to sham-operated controls. In sham-operated controls, the immunoreactivity of synapsin I is

evenly distributed in the whole hippocampus except the layer containing neuronal body (K). No obvious change in synapsin-I immunoreactivity is detected in the hippocampus in ischemic rats (L – O).

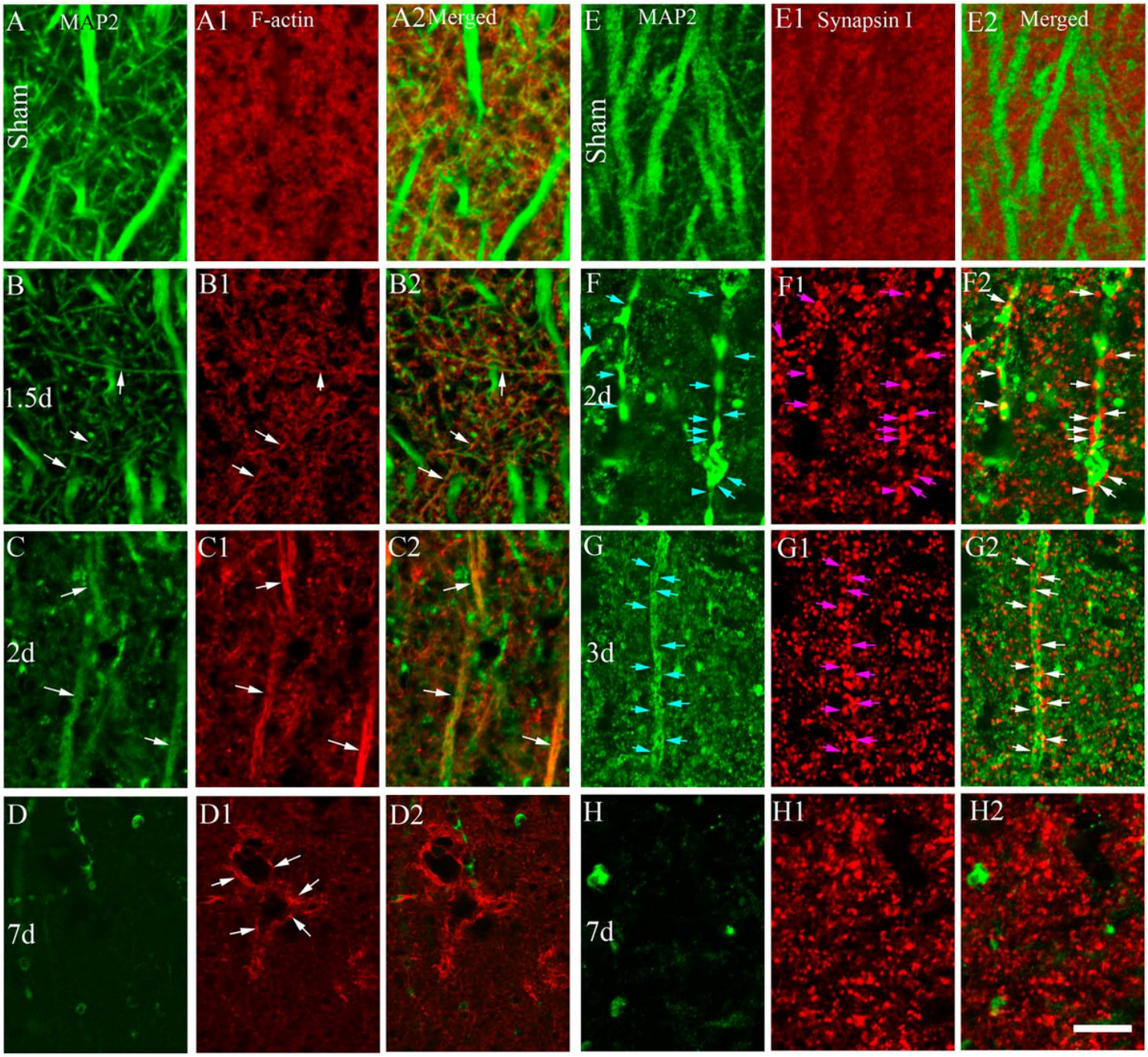

Figure 3

Double fluorescence labeling showing the localization of MAP2, F-actin, and synapsin I in CA1 stratum radiatum. Scale bars: 10μm. Sham-operated controls and different ischemic groups are labeled in the left-most column. The CA1 stratum radiatum is labeled for MAP2 (green, A-D, and E-H), F-actin (red, A1-D1), and synapsin I (E1-H1). Images in A2-D2 are merged from A-D and A1-D1, respectively. Images in E2-H2 are merged from E-H and E1-H1, respectively.

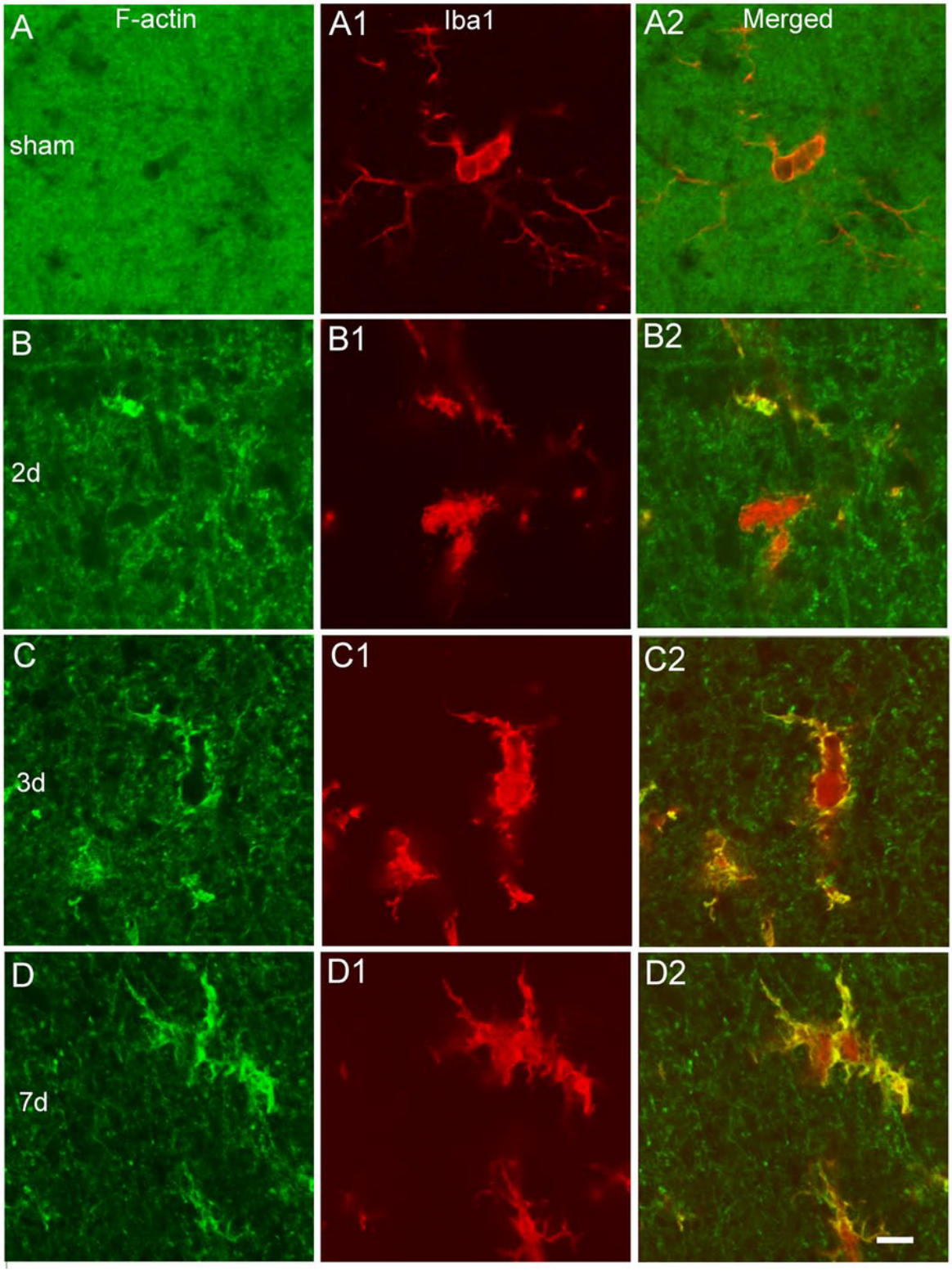

Figure 4

4 Double fluorescence labeling of F-actin (green) and Iba1 (red) in CA1 stratum radiatum after ischemia. Scale bars: 25 μm. CA1 stratum radiatum was evaluated by phalloidin staining for F-actin (green, A-D) and immunostaining against Iba1 (red, A1-D1) in the sham-operated control and ischemic animals on days 2, 3 and 7. Images in A2 – D2 are merged from A-D and A1-D1, respectively.

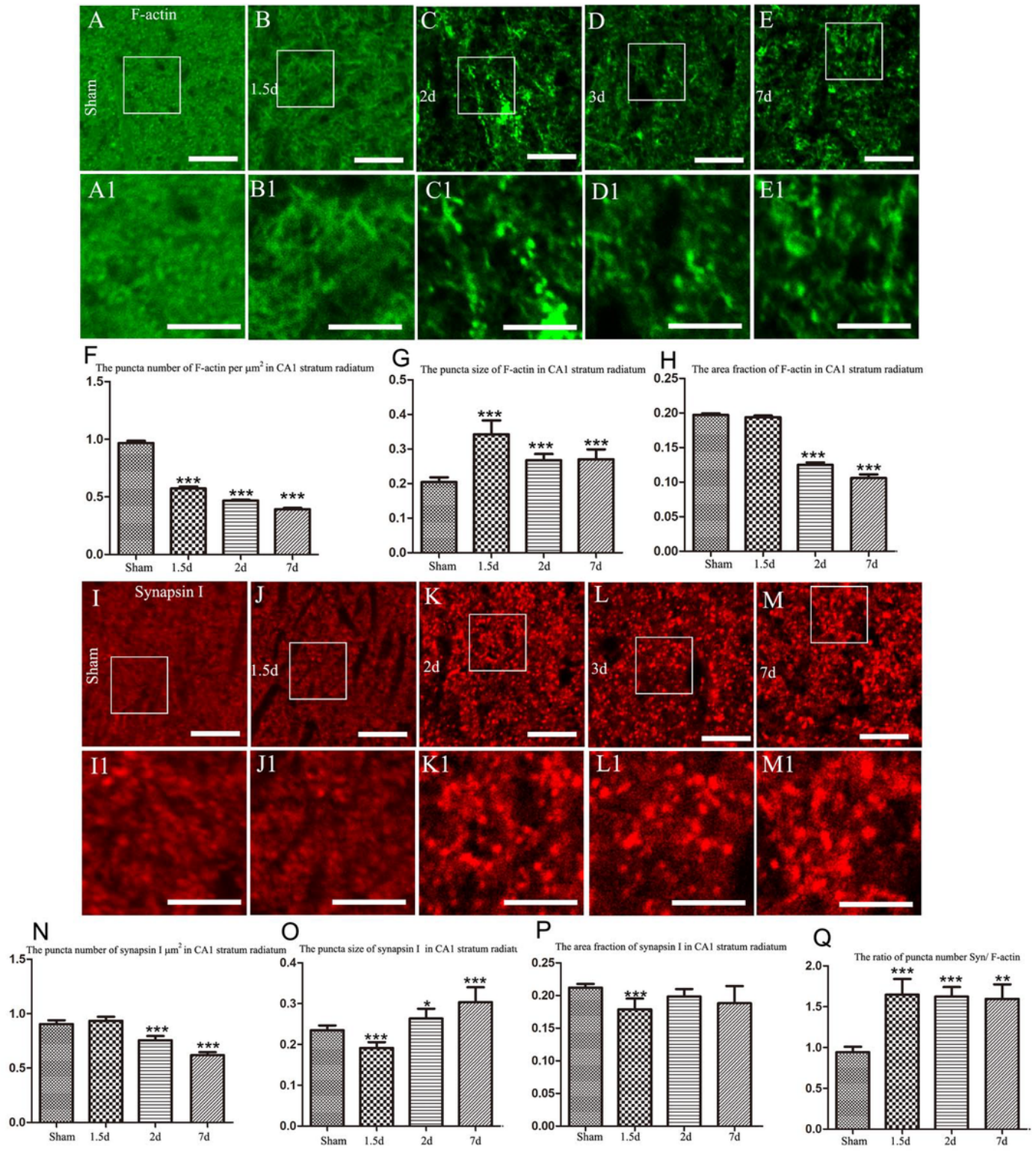

Figure 5

Quantitative analysis of fluorescence staining against F-actin and synapsin I. Scale bars: A-E, and I-M, 10μm; A1-E1, and I1-M1, 2.5μ. A-E show the distribution of F-actin in CA1 stratum radiatum in the sham-operated control (A) and ischemic animals on day 1.5 (B), 2 (C), 3 (D), and 7 (E), respectively. The insets in A - E are enlarged in A1 - E1, respectively. F - H show puncta number per unit area (F), mean puncta size (G) and mean area fraction (H) of F-actin in CA1 stratum radiatum, respectively (*P<0.05, ***P < 0.001

relative to the sham control, n=6 per group, Error bars represent SEM). I-M show the distribution of synapsin I in CA1 stratum radiatum in the sham-operated control (I) and ischemic animals at day 1.5 (I), 2 (K), 3 (L) and 7 (M), respectively. The insets in I - M are enlarged in I1 - M1, respectively. N - P show puncta number per unit area (N), mean puncta size (O) and mean area fraction (P) of synapsin I in CA1 stratum radiatum, respectively (***P < 0.001 relative to the sham control, n=6 per group, Error bars represent SEM). Q shows the ratio of synapsin I/F-actin puncta number (**P < 0.01, ***P < 0.001 relative to the sham control, n=6 per group, Error bars represent SEM).